

Electroweak Corrections at High Energies

Kalanand Mishra,¹ Luca Barzè,² Thomas Becher,³ Mauro Chiesa,⁴ Stefan Dittmaier,⁵ Xavier Garcia i Tormo,³ Alexander Huss,⁵ Tobias Kasprzik,⁶ Ye Li,⁷ Guido Montagna,⁴ Mauro Moretti,⁸ Oreste Nicrosini,⁴ Frank Petriello,^{9,10} Fulvio Piccinini,⁴ and Francesco Tramontano¹¹

¹*Fermi National Accelerator Laboratory, Batavia, IL 60510, USA*

²*CERN, PH-TH Department, Geneva, Switzerland*

³*Albert Einstein Center for Fundamental Physics, Institut für Theoretische Physik, Universität Bern, Sidlerstrasse 5, CH-3012 Bern, Switzerland*

⁴*Dipartimento di Fisica, Università di Pavia, and*

INFN, Sezione di Pavia, Via A. Bassi 6, 27100 Pavia, Italy

⁵*Albert-Ludwigs-Universität Freiburg, Physikalisches Institut, D-79104 Freiburg, Germany*

⁶*Karlsruhe Institute of Technology, Institut für Theoretische Teilchenphysik, D-76128 Karlsruhe, Germany*

⁷*SLAC National Accelerator Laboratory, Stanford University, Stanford, CA 94309, USA*

⁸*Dipartimento di Fisica e Scienze della Terra, Università di Ferrara, and*

INFN, Sezione di Ferrara, Via Saragat 1, 44100 Ferrara, Italy

⁹*High Energy Physics Division, Argonne National Laboratory, Argonne, IL 60439, USA*

¹⁰*Department of Physics & Astronomy, Northwestern University, Evanston, IL 60208, USA*

¹¹*Dipartimento di Scienze Fisiche, Università di Napoli “Federico II”, and*

INFN, Sezione di Napoli, via Cintia, 80126 Napoli, Italy

We present a survey of the most abundant processes at the LHC for sensitivity to electroweak corrections at $\sqrt{s} = 8, 14, 33$, and 100 TeV proton-proton collision energies. The processes studied are $pp \rightarrow$ dijet, inclusive W and Z, W/Z+jets, and WW. In each case we compare the experimental uncertainty in the highest kinematic regions of interest with the relative magnitude of electroweak corrections and fixed-order α_S calculations.

I. INTRODUCTION

At the Large Hadron Collider (LHC) design energy of 14 TeV and at future proton-proton (pp) colliders operating at even higher energies, the kinematic reach for the most abundant processes like dijet, inclusive W and Z, W/Z + jets, and vector-boson pair production will go deeper into the TeV regime and will become sensitive to electroweak (EW) corrections. In spite of their suppression by the small value of the coupling constant α , the EW corrections can become large in the high-energy domain due to the appearance of Sudakov logarithms that result from the virtual exchange of soft or collinear massive weak gauge bosons [1, 2]. The leading term is given by $\alpha_w \ln^2(Q^2/M_W^2)$, where Q denotes the energy scale of the hard-scattering process, M_W is the W-boson mass, and $\alpha_w = \alpha/\sin^2\theta_w = e^2/(4\pi\sin^2\theta_w)$ with θ_w denoting the weak mixing angle. In the case of massless gauge bosons, these logarithms are canceled by the corresponding real-emission corrections. However, the masses of the W and Z gauge bosons provide a physical cut-off. Therefore, radiation of real W or Z bosons can be experimentally reconstructed for the most part. Only a small fraction that remains unresolved can compensate for the virtual corrections [3]. Thus, at high scales $|Q^2| \gg M_W^2$, which are accessible at the LHC and future colliders, the Sudakov logarithms can produce large negative corrections. Although negligible for integrated cross sections, these corrections can reach 10–20% for transverse momentum (p_T) or invariant mass values in the TeV range. In this report, we study the evolution of EW corrections from the LHC to future high energy pp colliders for two benchmark values of collider energy, namely, 33 TeV and 100 TeV.

II. DIJET PRODUCTION

Inclusive production of two or more jets at the LHC allows for a detailed study of QCD at TeV energies. It is also the main background for searches of new heavy particles from beyond the Standard Model (SM) physics decaying into jets. Inclusive production of jets and dijets has been analyzed by the ATLAS [4] and CMS [5] collaborations at $\sqrt{s} = 7$ and 8 TeV. These measurements show sensitivity to dijet invariant masses of up to 5 TeV and jet transverse momenta of up to 2 TeV at the LHC. As shown in Fig. 1, at the current level of experimental and theoretical accuracy, the SM is able to describe data well. The size of the EW corrections is comparable to the experimental uncertainty for the highest p_T bins. In this respect the dijet measurements at $\sqrt{s} = 8$ TeV have already started probing the “Sudakov zone”. The EW corrections to dijet production shown in Fig. 1b are taken from Ref. [6]. These corrections comprise electroweak contributions of $\mathcal{O}(\alpha_s\alpha, \alpha^2)$

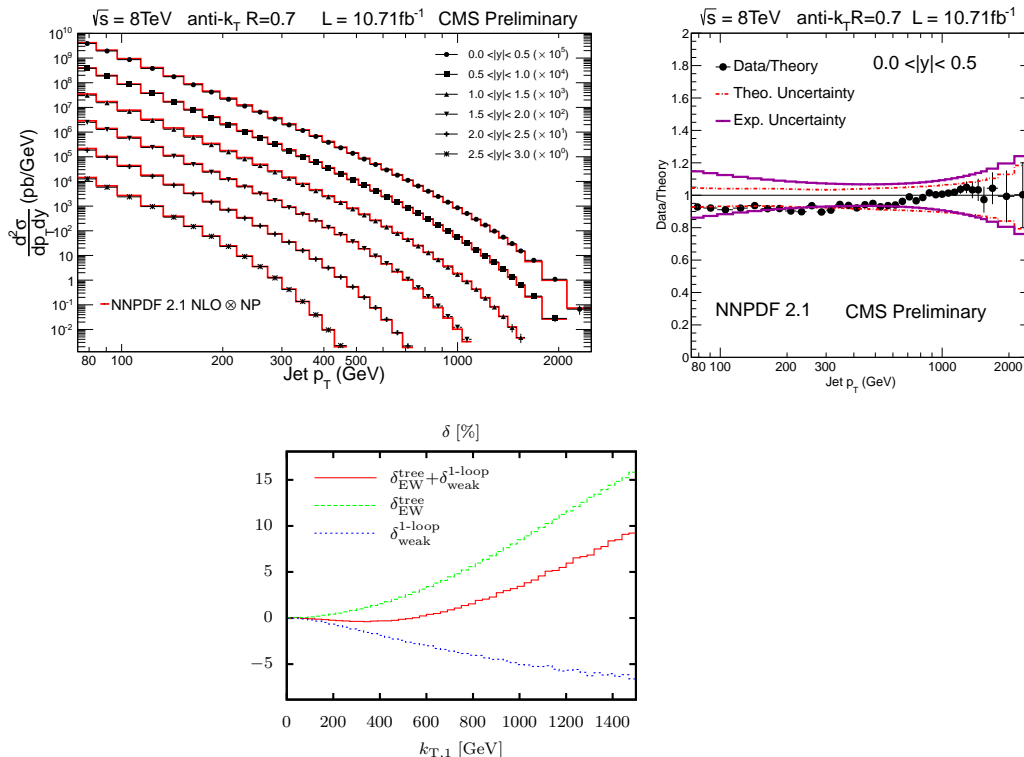


FIG. 1: The jet p_T spectrum measured in 8 TeV pp collisions (top left) along with uncertainties (top right) from Ref. [5]. Also shown is the relative magnitude of EW corrections at $\sqrt{s} = 8$ TeV (bottom) taken from Ref. [6].

to the leading-order (LO) QCD prediction as well as next-to-LO (NLO) corrections through the order $\alpha_s^2\alpha$. The tree-level contributions are of the same generic size as the loop corrections at $\sqrt{s} = 8$ TeV. The total correction to the integrated cross section is negligible, typically staying below the per-cent level. However, the Sudakov logarithms affect the tails of the distributions in the dijet invariant mass and in the transverse momenta of the two jets. The magnitude of the corrections at $\sqrt{s} = 8$ TeV and 14 TeV were found to be similar in Ref. [6]. Results from repeating the calculation for $\sqrt{s} = 33$ TeV and 100 TeV are shown in Fig. 2 and Fig. 3, respectively. We find that the 1-loop virtual corrections are not so dependent on the collider energy, while the tree-level corrections decrease with \sqrt{s} . Their cancellation is less perfect, and as a result, the virtual negative corrections dominate in the kinematic tails at large \sqrt{s} . Since the kinematic reach will increase with \sqrt{s} , these corrections will become progressively more important.

III. INCLUSIVE VECTOR BOSON PRODUCTION

The production of a single electroweak boson is one of the basic hard-scattering processes at the LHC and constitutes a major background to searches for physics beyond the SM, like $W' \rightarrow \ell\nu$ and $Z' \rightarrow \ell\ell$, and important SM measurements like $H \rightarrow ZZ^* \rightarrow 4\ell$. As in the dijet case, the EW corrections can become quite significant. Since we are considering single electroweak-boson production, without additional radiation of soft or collinear W or Z bosons, the cross section will contain Sudakov logarithms that can be as large as 20% for boson $p_T \sim 1$ TeV. These effects need to be included for precise predictions of kinematic distributions in the region $p_T \gg M_W$. Inclusive W and Z spectra have been analyzed by the ATLAS [7] and CMS [8] collaborations at $\sqrt{s} = 8$ TeV, showing sensitivity to boson invariant masses of up to 2 TeV and p_T of up to 800 GeV. As shown in Fig. 4, at the current level of experimental and theoretical accuracy, the SM is able to describe data well. The current experimental uncertainty for invariant masses above 1 TeV is somewhat larger than the size of the EW corrections. The same measurements at 14 TeV will be sensitive to probing the Sudakov zone.

For the above comparison we use Ref. [9] which provides a computation of EW Sudakov effects in single W, Z, and γ production at large boson p_T at $\sqrt{s} = 7$ TeV, with both QCD and electroweak effects included. Switching

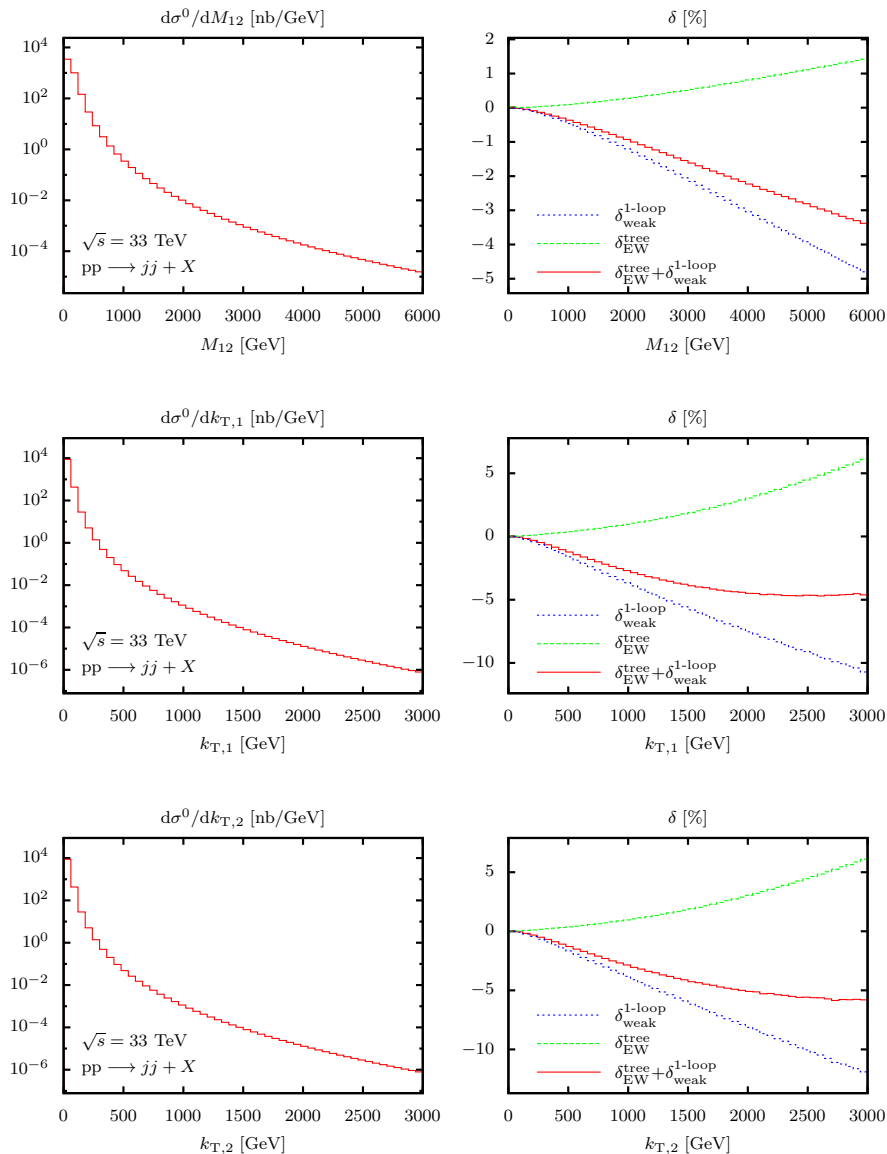


FIG. 2: Dijet production: Differential distributions with respect to the dijet invariant mass M_{12} (top), the transverse momentum of the leading jet $k_{T,1}$ (middle) and the sub-leading jet $k_{T,2}$ (bottom) at the pp collision energy of 33 TeV. Left: absolute predictions; right: relative contributions δ .

off the QCD effects, and expanding to NNLO, the results of Ref. [9] reproduce the earlier results [10, 11]. Results from repeating the same calculation for $\sqrt{s} = 33$ TeV and 100 TeV are shown in Fig. 5. We find that the relative corrections are basically independent of collider energy and depend only on p_T . However, as the kinematic reach increases with \sqrt{s} , these corrections will become more important.

A. Interplay of electroweak and QCD corrections in Drell-Yan production

The effects of electroweak Sudakov logarithms on more differential quantities, and their interplay with higher-order QCD corrections, are studied next for the example case of lepton-pair production via the Drell-Yan mechanism at a 33 TeV pp collider. The results shown are obtained with the numerical program FEWZ [12–14], which additively combines higher-order QCD and electroweak corrections. MSTW parton distribution

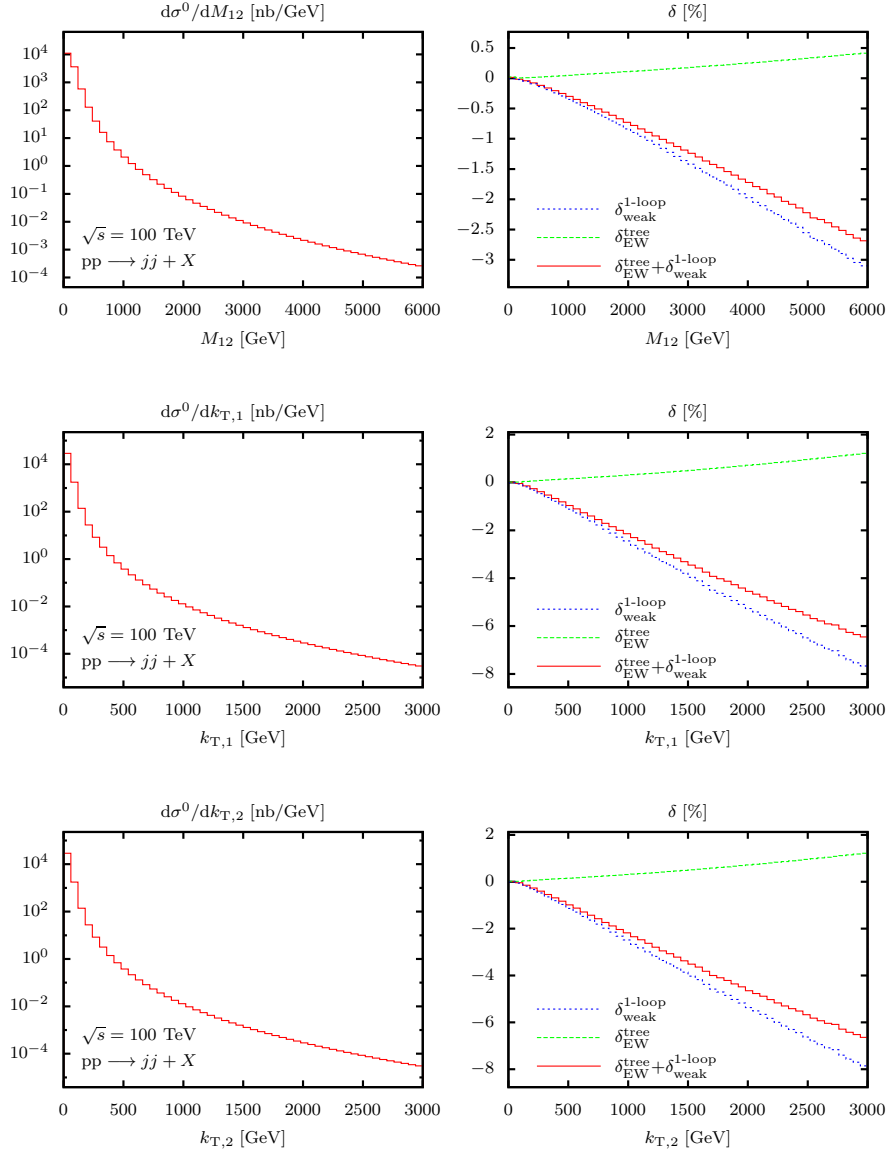


FIG. 3: Dijet production: Same distributions as in Fig. 2 for pp collision energy of 100 TeV.

functions [15] at the appropriate order in QCD perturbation theory are used. Shown first in Fig. 6 is the lepton-pair invariant mass distribution, with minimal acceptance cuts imposed on the transverse momenta and pseudorapidities of the leptons. The shift due to NLO QCD corrections alone is shown, as is the result of combining the full NLO electroweak correction with the QCD one. Both shifts are normalized to the leading-order prediction. Over a broad range of invariant masses, the QCD corrections increase the cross section by 20 – 30%. The electroweak corrections grow in importance with invariant mass, and lead to a decrease in the cross section. The electroweak corrections begin to overtake the QCD ones at $M_{ll} \approx 5$ TeV. The reduction in the cross section induced by the combined corrections reaches 20% at invariant masses of 15 TeV. Measurements of Drell-Yan production in 33 TeV collisions will be sensitive to the Sudakov zone over a large fraction of the available invariant mass range.

The shifts induced by the combined QCD and electroweak corrections on the lepton differential distributions are considered next. The cross section is first divided into the following invariant mass bins: $M_{ll} \in [500 \text{ GeV}, 1 \text{ TeV}]$, $M_{ll} \in [1 \text{ TeV}, 5 \text{ TeV}]$, and $M_{ll} \in [5 \text{ TeV}, 20 \text{ TeV}]$. The lepton transverse momentum and pseudorapidity distributions in each bin are then studied. The results are shown in Figs. 7, 8, and 9.

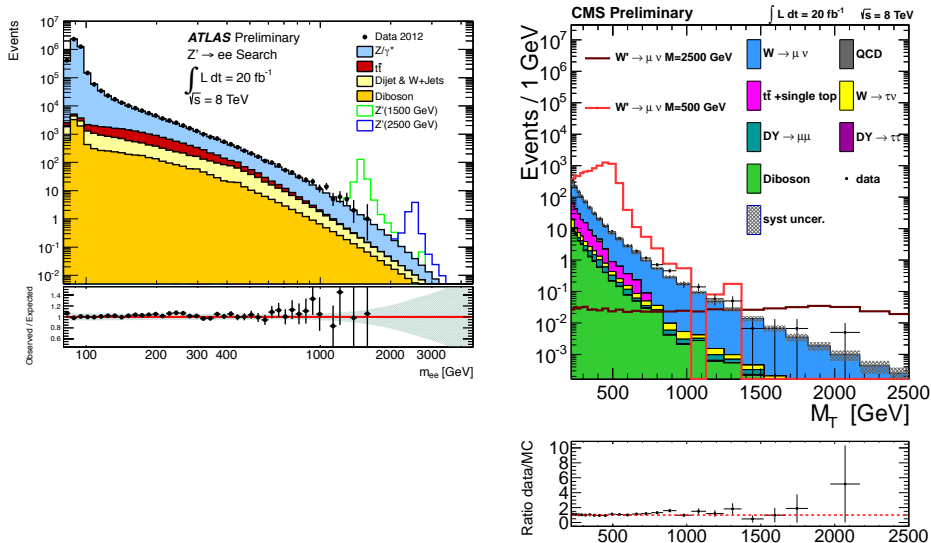


FIG. 4: Inclusive vector boson production: Observed vector-boson invariant mass distributions in 8 TeV pp collisions compared to the SM expectation (left) in events containing two energetic electrons. See Ref. [7] for details. On the right, the transverse mass distribution of the muon + missing transverse energy (E_T^{miss}) system is shown for events containing a high p_T muon and large E_T^{miss} . See Ref. [8] for details.

The QCD and electroweak corrections have the same shape as a function of lepton p_T . The dips appearing in the corrections at half the lower bin edge, and the rise at the upper bin edge, are artifacts of the Jacobian peaks present in the leading-order result. An interesting feature emerges in the lepton η distributions at higher invariant masses. The electroweak corrections act more strongly for central pseudorapidities, leading to a dip in the combined corrections that is quite large for the highest invariant mass bin. Large negative shifts in inclusive observables such as the vector-boson transverse momentum or invariant mass are not the only effects in the Sudakov zone. Distortions in the lepton η also occur because of the shape differences between QCD and electroweak corrections.

IV. VECTOR BOSON PRODUCTION IN ASSOCIATION WITH JETS

Production of a W or Z boson in association with jets has played a special role in collider physics. It was the dominant background to top-quark pair production at the Tevatron. At the LHC, it remains an important background for processes containing a lepton, missing energy (E_T^{miss}), and one or more jets in the final state. Prominent examples are measurements of top quark, Higgs boson, and multi-boson production and searches for supersymmetry signatures. Such measurements also permit stringent tests of the predictions of the SM. Measurements of W and Z boson production in association with multiple jets have been made by the ATLAS [16–18] and CMS [19–21] collaborations at $\sqrt{s} = 7$ and 8 TeV. These measurements show sensitivity to boson and leading-jet p_T of up to about 500 GeV at the LHC. As shown in Fig. 10, at the current level of experimental and theoretical accuracy, the SM is able to describe data well. The current experimental uncertainty for the highest p_T bins is somewhat larger than the size of the EW corrections. The same measurements at 14 TeV will be sensitive to probing the Sudakov zone.

Production cross sections for W + up to 5 jets and Z + up to 3 jets are now known at NLO QCD [22, 23]. The full NLO EW corrections for W + 1-jet production have been computed for the final state containing a charged lepton, a neutrino, and a hard jet [24], and for the monojet scenarios where the Z boson decays into two undetected neutrinos [25]. The full NLO EW corrections for Z + 1-jet production have also been computed for

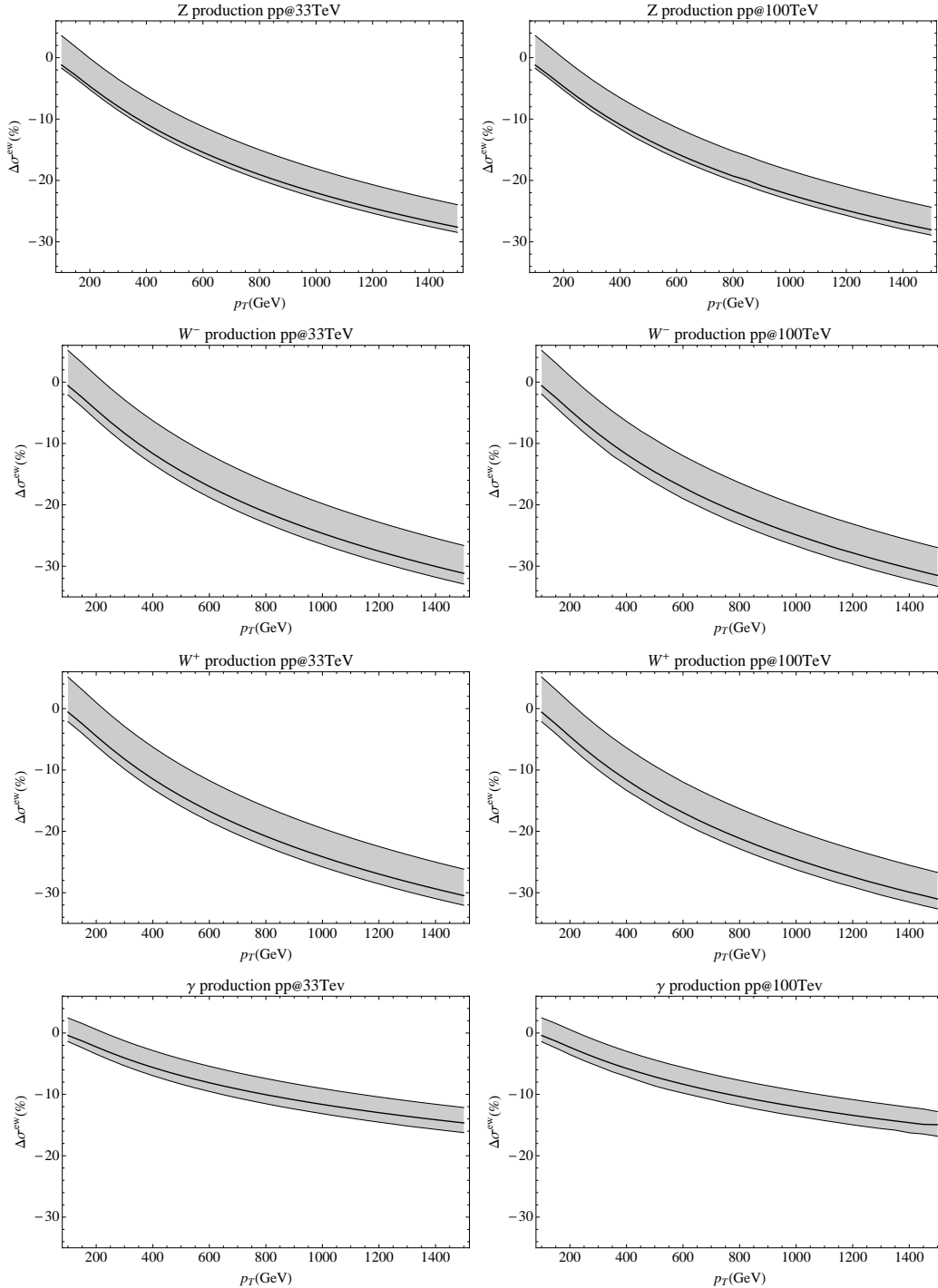


FIG. 5: Inclusive vector boson production: Relative contribution from EW corrections as a function of the vector boson p_T for Z (row 1), W^- (row 2), W^+ (row 3), and γ (row 4). Left: at the pp collision energy of 33 TeV; right: at 100 TeV.

the final state containing two charged leptons and a hard jet [26]. The overall magnitude of these corrections as a function of the boson p_T is similar to the inclusive W/Z case. Results from repeating the same calculation as in Ref. [26] for Z + 1-jet process at $\sqrt{s} = 33$ TeV are listed in Tables I and II as a function of the leading jet p_T and dilepton invariant mass, respectively. Corresponding results for $\sqrt{s} = 100$ TeV are listed in Tables III and IV. We find that the relative corrections show very weak dependence on \sqrt{s} and depend mostly on the jet (or boson) p_T and the invariant mass of the boson system. However, as the kinematic reach increases with \sqrt{s} , these corrections will become more important.

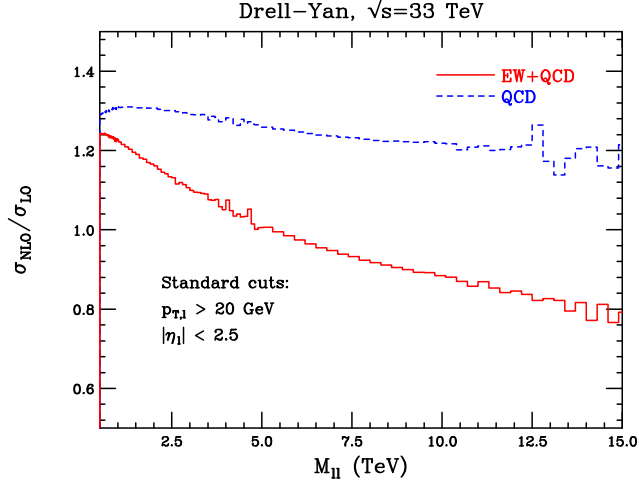


FIG. 6: Inclusive vector boson production: QCD corrections and combined electroweak-QCD corrections to lepton-pair production as a function of the lepton-pair invariant mass, at a 33 TeV pp collider.

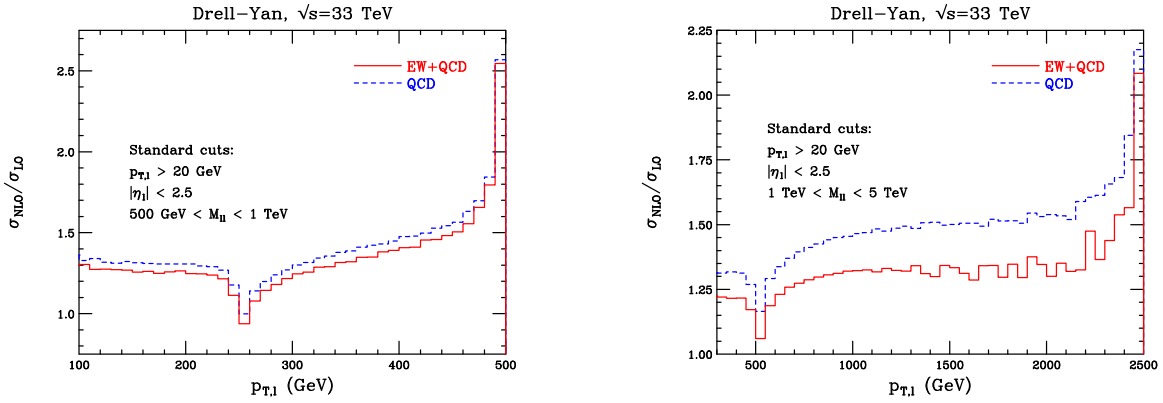


FIG. 7: Inclusive vector boson production: QCD corrections and combined electroweak-QCD corrections to lepton-pair production as a function of the lepton transverse momentum, at a 33 TeV pp collider. Results for two bins of lepton-pair invariant mass, $M_{ll} \in [500 \text{ GeV}, 1 \text{ TeV}]$, and $M_{ll} \in [1 \text{ TeV}, 5 \text{ TeV}]$, are shown.

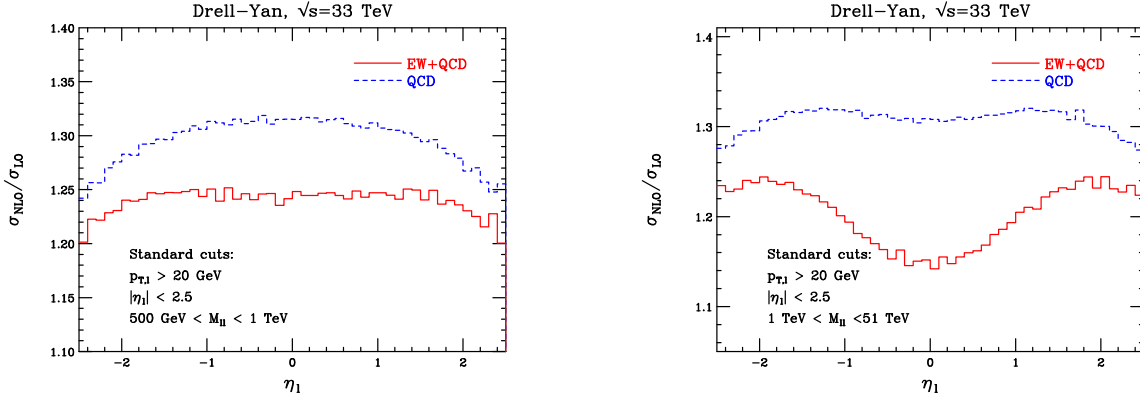


FIG. 8: Inclusive vector boson production: QCD corrections and combined electroweak-QCD corrections to lepton-pair production as a function of the lepton pseudorapidity, at a 33 TeV pp collider. Results for two bins of lepton-pair invariant mass $M_{II} \in [500 \text{ GeV}, 1 \text{ TeV}]$, and $M_{II} \in [1 \text{ TeV}, 5 \text{ TeV}]$, are shown.

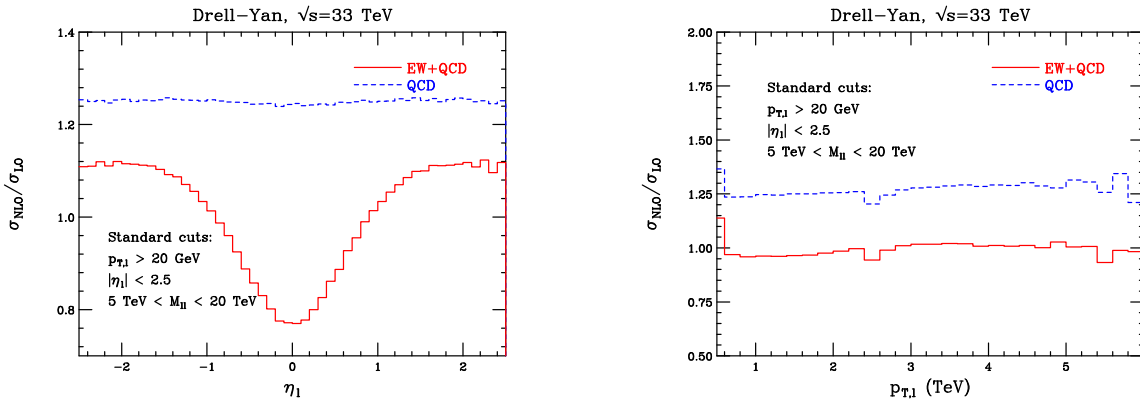


FIG. 9: Inclusive vector boson production: QCD corrections and combined electroweak-QCD corrections to lepton-pair production as a function of the lepton pseudorapidity and transverse momentum, at a 33 TeV pp collider. Results for the bin of lepton-pair invariant mass $M_{II} \in [5 \text{ TeV}, 20 \text{ TeV}]$ are shown

A. Z production in association with two and three jets

The virtual NLO EW Sudakov logarithmic corrections to vector bosons plus jets have been implemented in ALPGEN [27] through the algorithm of Refs. [28, 29], with phenomenological results for $Z + 2$ and $Z + 3$ jets production at LHC (at 7 and 14 TeV). Here we present the scaling of the corrections with the center of mass (c.m.) energy of proton-proton collisions from 14 TeV to 33 and 100 TeV. The event selections, parameters

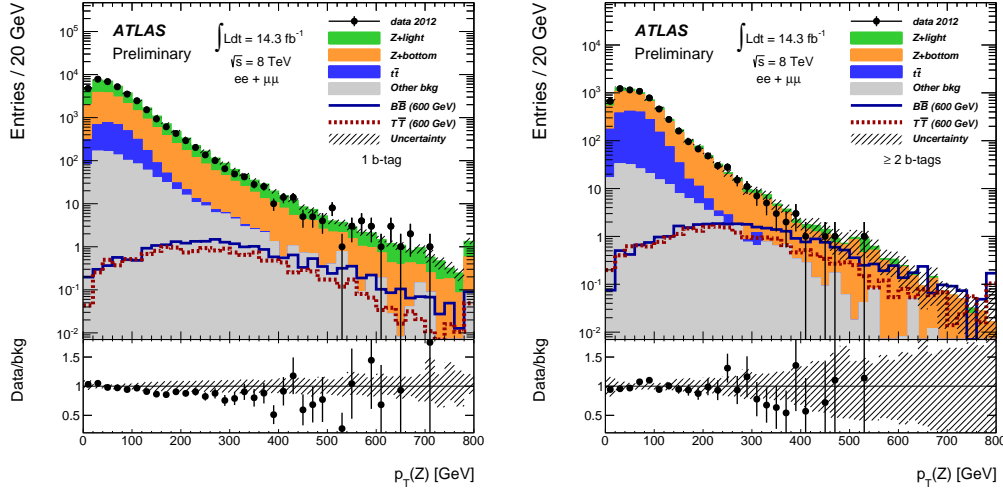


FIG. 10: Vector boson production in association with jets: Observed Z boson transverse momentum distribution in events containing at least two jets at $\sqrt{s} = 8$ TeV. (left) Exactly one jet is b-tagged. (right) At least two jets are b-tagged. For details see Ref. [18].

$pp \rightarrow l^+l^- \text{ jet} + X$ at $\sqrt{s} = 33$ TeV						
$p_{T,\text{jet}}/\text{GeV}$	50 – ∞	100 – ∞	200 – ∞	400 – ∞	1000 – ∞	2000 – ∞
$\sigma_{\text{Born}}^{\mu=M_Z}/\text{pb}$	121.26(1)	33.737(4)	6.3314(7)	0.79429(9)	0.026920(2)	0.0010264(1)
$\sigma_{\text{Born}}^{\text{var}}/\text{pb}$	120.70(1)	32.654(4)	5.6403(7)	0.60157(6)	0.014491(1)	0.00038663(4)
$\delta_{\text{EW}}^{\mu=M_Z}/\%$	-4.68(1)	-5.47(1)	-9.25(1)	-16.15(2)	-29.25(5)	-41.8(2)
$\delta_{\text{EW}}^{\text{rec},\mu=M_Z}/\%$	-3.29(3)	-4.48(2)	-8.50(4)	-15.42(3)	-28.59(8)	-41.0(1)
$\delta_{\text{EW}}^{\text{var}}/\%$	-4.61(1)	-5.31(1)	-8.92(1)	-15.65(2)	-28.48(5)	-40.5(3)
$\delta_{\text{EW}}^{\text{rec,var}}/\%$	-3.16(3)	-4.42(4)	-8.12(2)	-14.89(2)	-27.62(5)	-39.9(1)
$\delta_{\text{QCD}}^{\mu=M_Z}/\%$	56.1(2)	78.7(1)	113.0(1)	160.5(1)	240.4(2)	330.6(3)
$\delta_{\text{QCD}}^{\text{var}}/\%$	54.0(1)	77.4(1)	117.3(1)	186.0(1)	347.2(2)	609.0(4)
$\delta_{\text{QCD,veto}}^{\mu=M_Z}/\%$	13.1(1)	23.3(1)	29.7(1)	27.5(1)	-2.8(1)	-42.2(1)
$\delta_{\text{QCD,veto}}^{\text{var}}/\%$	12.9(1)	25.6(2)	38.8(1)	49.8(1)	52.6(1)	54.0(1)
$\delta_{\gamma,\text{Born}}^{\mu=M_Z}/\%$	0.1377(4)	0.1647(4)	0.1960(5)	0.2442(7)	0.341(1)	0.457(1)
$\delta_{\gamma,\text{Born}}^{\text{var}}/\%$	0.1489(4)	0.1923(5)	0.2562(7)	0.371(1)	0.661(2)	1.095(3)
$\sigma_{\text{full,veto}}^{\text{var}}/\text{pb}/\%$	130.9(2)	39.36(6)	7.342(9)	0.8091(7)	0.01808(2)	0.000443(1)

TABLE I: Z + 1-jet production: Integrated cross sections for different cuts on the p_T of the leading jet (jet with highest p_T) at a pp collider with $\sqrt{s} = 33$ TeV. The LO results are shown both for a variable and for a constant scale. The relative EW corrections δ_{EW} are given with and without lepton-photon recombination. The QCD corrections δ_{QCD} are presented for a fixed as well as for a variable scale and with or without employing a veto on a second hard jet. The EW corrections and the corrections due to photon-induced processes, δ_{γ} , are presented for the variable scale. Finally, the last row shows the full NLO cross section $\sigma_{\text{full,veto}}^{\text{var}}$. The error from the Monte Carlo integration for the last digit(s) is given in parenthesis. See Ref. [26] for details.

and considered observables are those of Ref. [27]. The parameters and PDF setting are the ALPGEN defaults. In particular, for Z + 2 jets, we consider the observables/cuts presently adopted by ATLAS [30], namely

$$\begin{aligned}
 m_{\text{eff}} &> 1 \text{ TeV} & \cancel{E}_T/m_{\text{eff}} &> 0.3 \\
 p_T^{j_1} &> 130 \text{ GeV} & p_T^{j_2} &> 40 \text{ GeV} & |\eta_j| &< 2.8 \\
 \Delta\phi(\vec{p}_T^j, \vec{\cancel{E}}_T) &> 0.4 & \Delta R_{(j_1, j_2)} &> 0.4
 \end{aligned} \tag{1}$$

pp $\rightarrow l^+l^-$ jet + X at $\sqrt{s} = 33$ TeV					
M_{ll}/GeV	100 – ∞	200 – ∞	400 – ∞	1000 – ∞	2000 – ∞
$\sigma_{\text{Born}}^{\mu=M_Z}/\text{pb}$	19.924(6)	1.6890(2)	0.28005(4)	0.022682(3)	0.0024968(4)
$\sigma_{\text{Born}}^{\text{var}}/\text{pb}$	19.849(6)	1.6482(2)	0.26618(4)	0.020604(3)	0.0021755(3)
$\delta_{\text{EW}}^{\mu=M_Z}/\%$	-9.6(1)	-5.74(1)	-8.26(1)	-14.31(2)	-21.69(3)
$\delta_{\text{EW}}^{\text{rec},\mu=M_Z}/\%$	-5.3(1)	-3.06(1)	-5.13(1)	-10.11(2)	-16.34(3)
$\delta_{\text{EW}}^{\text{var}}/\%$	-9.46(8)	-5.69(1)	-8.14(1)	-14.18(2)	-21.56(3)
$\delta_{\text{EW}}^{\text{rec,var}}/\%$	-5.05(7)	-2.94(1)	-4.93(1)	-9.93(2)	-16.14(3)
$\delta_{\text{QCD}}^{\mu=M_Z}/\%$	29.(1)	14.8(2)	-0.6(1)	-29.5(1)	-57.1(1)
$\delta_{\text{QCD}}^{\text{var}}/\%$	27.9(6)	15.9(2)	2.2(1)	-23.0(1)	-46.6(1)
$\delta_{\text{QCD,veto}}^{\mu=M_Z}/\%$	5.0(6)	-8.9(2)	-25.5(1)	-54.9(1)	-82.4(1)
$\delta_{\text{QCD,veto}}^{\text{var}}/\%$	6.1(4)	-7.2(2)	-20.8(2)	-45.8(1)	-69.8(1)
$\delta_{\gamma,\text{Born}}^{\mu=M_Z}/\%$	0.669(1)	2.097(5)	2.409(6)	2.168(6)	1.844(5)
$\delta_{\gamma,\text{Born}}^{\text{var}}/\%$	0.710(1)	2.298(5)	2.721(7)	2.510(7)	2.135(5)
$\sigma_{\text{full,veto}}^{\text{var}}/\text{pb}/\%$	19.32(9)	1.473(4)	0.1965(6)	0.00877(2)	0.000234(3)

TABLE II: Z + 1-jet production: Integrated cross sections for different cuts on the dilepton invariant mass at a pp collider with $\sqrt{s} = 33$ TeV. See caption of Table I and text for details.

pp $\rightarrow l^+l^-$ jet + X at $\sqrt{s} = 100$ TeV						
$p_{T,\text{jet}}/\text{GeV}$	100 – ∞	200 – ∞	400 – ∞	800 – ∞	2000 – ∞	4000 – ∞
$\sigma_{\text{Born}}^{\mu=M_Z}/\text{pb}$	114.29(1)	23.772(3)	3.5452(4)	0.42003(4)	0.017238(1)	0.00094403(9)
$\sigma_{\text{Born}}^{\text{var}}/\text{pb}$	118.30(1)	23.762(3)	3.1922(3)	0.31583(3)	0.0091290(9)	0.00035205(3)
$\delta_{\text{EW}}^{\mu=M_Z}/\%$	-5.62(1)	-9.57(1)	-16.86(2)	-27.11(8)	-43.5(1)	-58.8(1)
$\delta_{\text{EW}}^{\text{rec},\mu=M_Z}/\%$	-4.65(3)	-8.72(2)	-16.08(2)	-26.29(4)	-43.15(7)	-58.5(2)
$\delta_{\text{EW}}^{\text{var}}/\%$	-5.50(1)	-9.29(1)	-16.38(3)	-26.36(4)	-43.2(2)	-57.5(1)
$\delta_{\text{EW}}^{\text{rec,var}}/\%$	-4.48(2)	-8.52(2)	-15.62(2)	-25.64(4)	-42.21(7)	-56.8(1)
$\delta_{\text{QCD}}^{\mu=M_Z}/\%$	97.4(2)	146.0(1)	215.2(2)	288.7(2)	378.0(3)	472.6(5)
$\delta_{\text{QCD}}^{\text{var}}/\%$	85.4(2)	130.0(2)	201.7(1)	298.8(2)	487.9(3)	769.0(7)
$\delta_{\text{QCD,veto}}^{\mu=M_Z}/\%$	35.7(2)	54.2(1)	66.7(1)	61.3(1)	13.2(2)	-43.1(1)
$\delta_{\text{QCD,veto}}^{\text{var}}/\%$	29.6(2)	47.4(1)	65.5(1)	76.4(3)	65.6(2)	51.5(1)
$\delta_{\gamma,\text{Born}}^{\mu=M_Z}/\%$	0.1218(3)	0.1400(4)	0.1681(5)	0.2114(7)	0.291(1)	0.382(1)
$\delta_{\gamma,\text{Born}}^{\text{var}}/\%$	0.1407(3)	0.1799(5)	0.2482(7)	0.365(1)	0.630(2)	1.006(5)
$\sigma_{\text{full,veto}}^{\text{var}}/\text{pb}/\%$	147.0(2)	32.86(4)	4.767(4)	0.475(1)	0.01124(2)	0.0003343(7)

TABLE III: Z + 1-jet production: Integrated cross sections for different cuts on the p_T of the leading jet at a pp collider with $\sqrt{s} = 100$ TeV. See caption of Table I and text for details.

where j_1 and j_2 are the leading and next-to-leading p_T jets; $m_{\text{eff}} = \sum_i p_{T_i} + \cancel{E}_T$.

For the Z + 3 jets final state we consider the observables/cuts used by CMS [31, 32], namely

$$\begin{aligned}
H_T &> 500 \text{ GeV} & |\vec{\cancel{H}}_T| &> 200 \text{ GeV} \\
p_T^j &> 50 \text{ GeV} & |\eta_j| &< 2.5 & \Delta R_{(j_i,j_k)} &> 0.5 \\
\Delta\phi(\vec{p}_T^{j_1,j_2}, \vec{\cancel{H}}_T) &> 0.5 & \Delta\phi(\vec{p}_T^{j_3}, \vec{\cancel{H}}_T) &> 0.3,
\end{aligned} \tag{2}$$

where $H_T = \sum_i p_{T_i}$ and $\vec{\cancel{H}}_T = -\sum_i \vec{p}_{t_i}$. For the sake of reference, we report here some partial results from Ref. [27] corresponding to the c.m. energy of 14 TeV.

pp $\rightarrow l^+l^-$ jet + X at $\sqrt{s} = 100$ TeV					
M_{ll}/GeV	100 - ∞	200 - ∞	400 - ∞	1000 - ∞	2000 - ∞
$\sigma_{\text{Born}}^{\mu=M_Z}/\text{pb}$	60.70(2)	5.3194(9)	0.9142(1)	0.08462(1)	0.012762(2)
$\sigma_{\text{Born}}^{\text{var}}/\text{pb}$	61.76(2)	5.3548(9)	0.9016(1)	0.07980(1)	0.011500(2)
$\delta_{\text{EW}}^{\mu=M_Z}/\%$	-9.4(1)	-5.85(1)	-8.41(1)	-14.28(2)	-21.05(3)
$\delta_{\text{EW}}^{\text{rec},\mu=M_Z}/\%$	-5.0(1)	-3.23(1)	-5.29(1)	-10.42(3)	-16.42(3)
$\delta_{\text{EW}}^{\text{var}}/\%$	-9.5(2)	-5.76(1)	-8.31(1)	-14.08(2)	-20.85(3)
$\delta_{\text{EW}}^{\text{rec,var}}/\%$	-5.2(2)	-3.07(1)	-5.15(2)	-10.11(2)	-16.22(4)
$\delta_{\text{QCD}}^{\mu=M_Z}/\%$	36.(4)	20.8(3)	7.3(2)	-18.1(1)	-43.3(1)
$\delta_{\text{QCD}}^{\text{var}}/\%$	29.3(9)	18.4(3)	6.0(1)	-16.3(1)	-37.4(1)
$\delta_{\text{QCD,veto}}^{\mu=M_Z}/\%$	5.0(9)	-7.0(2)	-21.2(2)	-46.8(1)	-71.8(1)
$\delta_{\text{QCD,veto}}^{\text{var}}/\%$	3.8(7)	-7.4(3)	-19.6(2)	-41.7(1)	-63.1(1)
$\delta_{\gamma,\text{Born}}^{\mu=M_Z}/\%$	0.532(1)	1.679(4)	2.019(6)	1.988(6)	1.792(6)
$\delta_{\gamma,\text{Born}}^{\text{var}}/\%$	0.568(1)	1.871(4)	2.363(7)	2.464(7)	2.259(7)
$\sigma_{\text{full,veto}}^{\text{var}}/\text{pb}/\%$	58.6(4)	4.75(1)	0.672(1)	0.0373(1)	0.00211(2)

TABLE IV: Z + 1-jet production: Integrated cross sections for different cuts on the dilepton invariant mass at a pp collider with $\sqrt{s} = 100$ TeV. See caption of Table I and text for details.

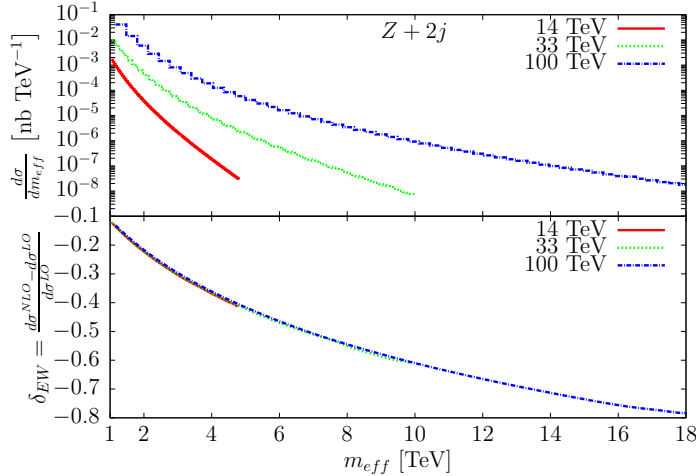


FIG. 11: Z + 2 jets: $d\sigma/dm_{\text{eff}}$ (absolute LO predictions and relative EW Sudakov corrections) at $\sqrt{s} = 14, 33$ and 100 TeV.

In Fig. 11 we show the absolute LO distribution $d\sigma/dm_{\text{eff}}$ and the relative effects of the Sudakov EW corrections corresponding to three different c.m. energies: 14, 33 and 100 TeV. As can be seen, the negative corrections due to Sudakov logs are of the order of some tens of per cent, raising to about 40% (60%, 80%) in the extreme regions at $\sqrt{s} = 14$ (33, 100) TeV, respectively. For a given bin of the m_{eff} distribution, the relative EW corrections are practically the same, independently of the collider c.m. energy.

In Fig. 12 we show the effect of the Sudakov logs on the observable $|\vec{H}_T|$ in the process $pp \rightarrow Z + 3$ jets according to the event selection of Eq. (2). As for the Z + 2 jets effective mass distributions, the effect of NLO weak corrections on $|\vec{H}_T|$ is large and negative, raising to about 40% (60%, 70%) in the extreme regions at $\sqrt{s} = 14$ (33, 100) TeV, respectively. For a chosen $|\vec{H}_T|$ bin, the relative effects of the corrections are quite insensitive to the change of the collider energy.

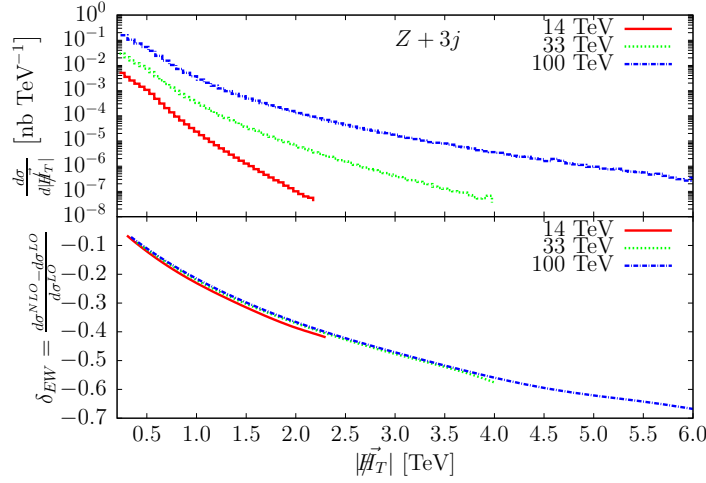


FIG. 12: $Z + 3$ jets: $d\sigma/|H_T|$ (absolute LO predictions and relative EW Sudakov corrections) at $\sqrt{s} = 14, 33$ and 100 TeV.

V. VECTOR-BOSON PAIR PRODUCTION

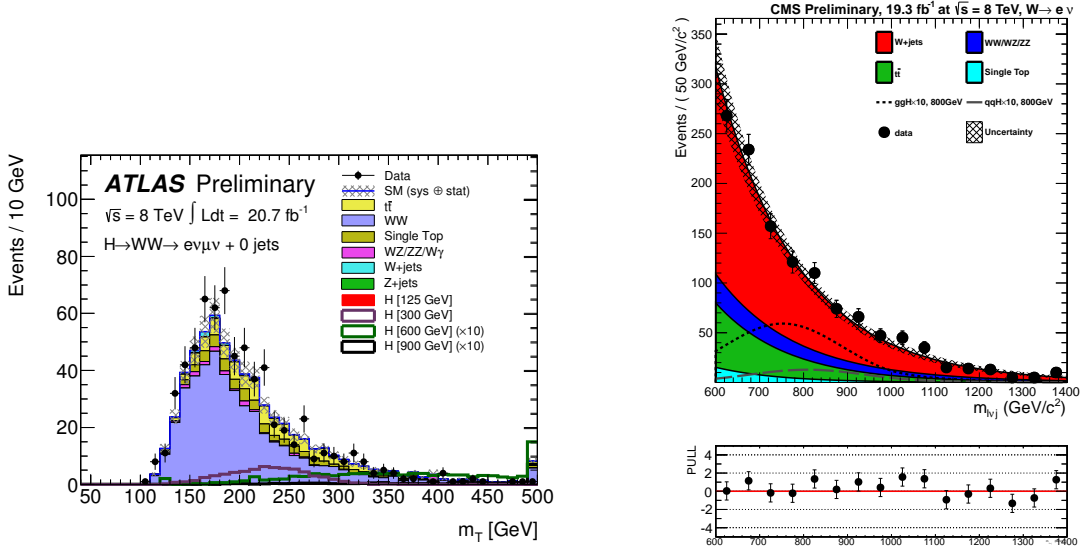


FIG. 13: Vector-boson pair production at $\sqrt{s} = 8$ TeV: (left) Observed transverse mass distribution of the WW system in the fully leptonic decay mode electron+muon+ \cancel{E}_T and no jet activity. For details see Ref. [33]. (b) Observed invariant mass distribution of the WW candidates in the semi-leptonic decay mode where one W boson decays leptonically to $e\nu$ and the other W boson decays at high p_T to $q\bar{q}$ giving rise to a single merged jet. For details see Ref. [34].

Vector-boson pair production is among the most important SM benchmark processes at the LHC because of its connection to electroweak symmetry breaking, to the study of Higgs boson in $H \rightarrow WW^*, ZZ^*, \gamma\gamma$ processes, and to probes of gauge boson self interactions. Diboson production can also provide a deeper understanding of the electroweak interactions in general, and to test the validity of the SM at the highest available energies.

In this report we focus on WW production at large invariant masses or large W p_T , which is the kinematic regime of high interest that can have large EW corrections. This kinematic regime has recently been analyzed by the ATLAS [33] and CMS [34] collaborations at $\sqrt{s} = 8$ TeV showing sensitivity to invariant masses of up to 1 TeV and boson transverse momenta of up to 500 GeV. Comparing with the full one-loop EW corrections to on-shell WW production [35] we find that the size of the correction is comparable to the experimental uncertainty for highest kinematic end points. As noted in Ref. [35], the corrections due to photon-induced

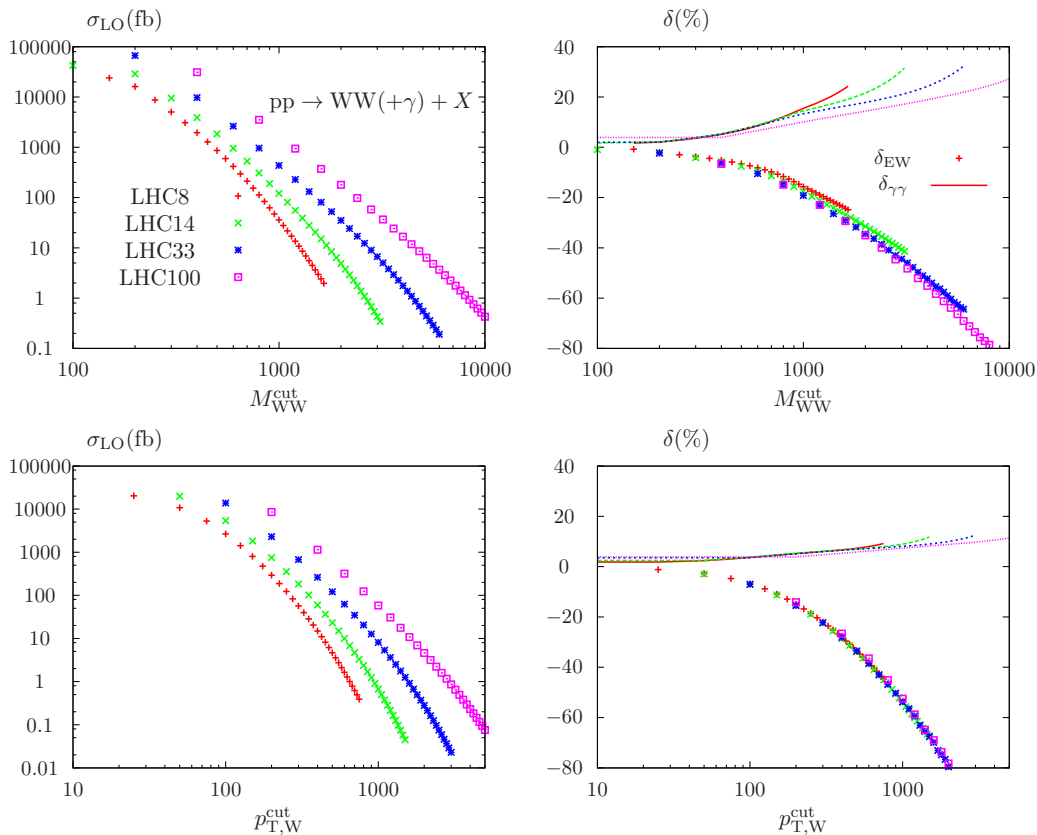


FIG. 14: WW production: Total cross sections for W-pair production for different cuts on WW invariant mass (top row) and W transverse momentum (bottom row), evaluated at pp collision energies of 8, 14, 33, and 100 TeV. Left: absolute predictions, right: relative electroweak corrections (δ_{EW}) and relative contributions from the $\gamma\gamma$ -induced process ($\delta_{\gamma\gamma}$).

channels can be large at high energies, while radiation of additional massive vector bosons does not influence the results significantly. Recently, a detailed study of vector-boson pair production at NLO has been presented in Ref. [36], where the authors emphasize the importance of photon-induced processes, which may potentially lead to significant distortions of differential distributions. Results from repeating the calculation from Ref. [35] for $\sqrt{s} = 33$ TeV and 100 TeV are shown in Fig. 14. We find that while the relative NLO EW corrections hardly depend on the collider energy, the relative photon-induced contributions are suppressed at larger values of \sqrt{s} . As a result, the overall corrections show very little dependence on \sqrt{s} . However, like in the case of other processes described earlier, the EW corrections will progressively become more important with increase in \sqrt{s} due to higher kinematic reach.

VI. SUMMARY

We have presented a survey of the most abundant processes at the LHC for sensitivity to electroweak corrections at various pp collision energies relevant for LHC and future hadron colliders. We summarize our observations in Table V. We find that for most processes the overall electroweak corrections do not change much with increase in collider energy. However, the corrections become more important at high collider energies simply because of the increase in kinematic reach at high \sqrt{s} , where the corrections are inherently large.

TABLE V: Are we in the Sudakov zone yet?

Process	$\sqrt{s} = 8 \text{ TeV}$	$\sqrt{s} = 14 \text{ TeV}$	$\sqrt{s} = 33, 100 \text{ TeV}$
Inclusive jet, dijet	Yes	Yes	Yes
Inclusive W/Z tail	\sim Yes	Yes	Yes
$W\gamma, Z\gamma$ tail ($\ell\nu\gamma, \ell\ell\gamma$)	No	\sim Yes	Yes
W/Z+jets tail	\sim Yes	Yes	Yes
WW leptonic	Close	\sim Yes	Yes
WZ, ZZ leptonic	No	No	Yes
WW, WZ, ZZ semileptonic	\sim Yes	Yes	Yes

VII. ACKNOWLEDGEMENTS

We would like to thank John Campbell, Kenichi Hatakeyama, Joey Huston, Michael Peskin, and Doreen Wackerroth for requesting these studies for Snowmass 2013 report and for providing valuable feedback. Fermilab is operated by Fermi Research Alliance, LLC, under Contract No. DE-AC02-07CH11359 with the United States Department of Energy. This work is supported in part by the Research Executive Agency (REA) of the European Union under the Grant Agreement number PITN-GA-2010-264564 (LHCPhenoNet), and by the Italian Ministry of University and Research under the 2010-2011 PRIN program 2010YJ2NYW. The work of L. B. is supported by the ERC grant 291377, ‘‘LHCtheory - Theoretical predictions and analyses of LHC physics: advancing the precision frontier’’. The work of T. B. and X. G. is supported by the Swiss National Science Foundation (SNF) under grant 200020-140978 and the Sinergia grant number CRSII2 141847 1. The work of F. Petriello is supported by the U.S. Department of Energy, Division of High Energy Physics, under contract DE-AC02-06CH11357 and the grant de-sc0010143.

-
- [1] V. V. Sudakov, Sov. Phys. JETP **3** (1956) 65.
[2] V. S. Fadin, L. N. Lipatov, A. D. Martin and M. Melles, Phys. Rev. D **61**, 094002 (2000) [hep-ph/9910338].
[3] U. Baur, Phys. Rev. D **75** (2007) 013005 [hep-ph/0611241].
[4] G. Aad *et al.* [ATLAS Collaboration], Phys. Rev. D **86**, 014022 (2012) [arXiv:1112.6297 [hep-ex]].
[5] CMS Collaboration, <https://cdsweb.cern.ch/record/1547589> (2013).
[6] S. Dittmaier, A. Huss and C. Speckner, JHEP **1211**, 095 (2012) [arXiv:1210.0438 [hep-ph]].
[7] ATLAS Collaboration, <http://cds.cern.ch/record/1525524> (2013).
[8] CMS Collaboration, <http://cds.cern.ch/record/1522476> (2013).
[9] T. Becher and X. G. iTormo, Phys. Rev. D **88**, 013009 (2013) [arXiv:1305.4202 [hep-ph]].
[10] J. H. Kuhn, A. Kulesza, S. Pozzorini and M. Schulze, Nucl. Phys. B **727**, 368 (2005) [hep-ph/0507178].
[11] J. H. Kuhn, A. Kulesza, S. Pozzorini and M. Schulze, Nucl. Phys. B **797**, 27 (2008) [arXiv:0708.0476 [hep-ph]].
[12] K. Melnikov and F. Petriello, Phys. Rev. D **74**, 114017 (2006) [hep-ph/0609070].
[13] R. Gavin, Y. Li, F. Petriello and S. Quackenbush, Comput. Phys. Commun. **182**, 2388 (2011) [arXiv:1011.3540 [hep-ph]].
[14] Y. Li and F. Petriello, Phys. Rev. D **86**, 094034 (2012) [arXiv:1208.5967 [hep-ph]].
[15] A. D. Martin, W. J. Stirling, R. S. Thorne and G. Watt, Eur. Phys. J. C **63**, 189 (2009) [arXiv:0901.0002 [hep-ph]].
[16] G. Aad *et al.* [ATLAS Collaboration], Phys. Rev. D **85**, 092002 (2012) [arXiv:1201.1276 [hep-ex]].
[17] G. Aad *et al.* [ATLAS Collaboration], Phys. Rev. D **85**, 032009 (2012) [arXiv:1111.2690 [hep-ex]].
[18] ATLAS Collaboration, <http://cds.cern.ch/record/1557773> (2013).
[19] S. Chatrchyan *et al.* [CMS Collaboration], JHEP **1201**, 010 (2012) [arXiv:1110.3226 [hep-ex]].
[20] S. Chatrchyan *et al.* [CMS Collaboration], JHEP **1206**, 126 (2012) [arXiv:1204.1643 [hep-ex]].
[21] CMS Collaboration, <https://cdsweb.cern.ch/record/1537320> (2013).
[22] C. F. Berger, Z. Bern, L. J. Dixon, F. Febres Cordero, D. Forde, T. Gleisberg, H. Ita and D. A. Kosower *et al.*, Phys. Rev. Lett. **106**, 092001 (2011) [arXiv:1009.2338 [hep-ph]].
[23] Z. Bern, L. J. Dixon, F. Febres Cordero, S. Hoeche, H. Ita, D. A. Kosower, D. Maitre and K. J. Ozeren, arXiv:1304.1253 [hep-ph].
[24] A. Denner, S. Dittmaier, T. Kasprzik and A. Muck, JHEP **0908**, 075 (2009) [arXiv:0906.1656 [hep-ph]].
[25] A. Denner, S. Dittmaier, T. Kasprzik and A. Mck, Eur. Phys. J. C **73** (2013) 2297 [arXiv:1211.5078 [hep-ph]].
[26] A. Denner, S. Dittmaier, T. Kasprzik and A. Muck, JHEP **1106**, 069 (2011) [arXiv:1103.0914 [hep-ph]].

- [27] M. Chiesa, G. Montagna, L. Barzè, M. Moretti, O. Nicrosini, F. Piccinini and F. Tramontano, arXiv:1305.6837 [hep-ph].
- [28] A. Denner and S. Pozzorini, Eur. Phys. J. C **18**, 461 (2001) [hep-ph/0010201].
- [29] A. Denner and S. Pozzorini, Eur. Phys. J. C **21**, 63 (2001) [hep-ph/0104127].
- [30] G. Aad *et al.* [ATLAS Collaboration], Phys. Lett. B **710**, 67 (2012) [arXiv:1109.6572 [hep-ex]].
- [31] S. Chatrchyan *et al.* [CMS Collaboration], JHEP **1108**, 155 (2011) [arXiv:1106.4503 [hep-ex]].
- [32] S. Chatrchyan *et al.* [CMS Collaboration], Phys. Rev. Lett. **109**, 171803 (2012) [arXiv:1207.1898 [hep-ex]].
- [33] ATLAS Collaboration, <http://cds.cern.ch/record/1562879> (2013).
- [34] CMS Collaboration, <http://cds.cern.ch/record/1546778> (2013).
- [35] A. Bierweiler, T. Kasprzik, H. Kuhn and S. Uccirati, JHEP **1211**, 093 (2012) [arXiv:1208.3147 [hep-ph]].
- [36] J. Baglio, L. D. Ninh and M. M. Weber, arXiv:1307.4331 [hep-ph].